Early-age hydration of accelerated low-carbon cements for digital fabrication

Cement and Concrete Composites 159 (2025) 105991

Contents lists available at ScienceDirect

Cement and Concrete Composites

journal homepage: www.elsevier.com/locate/cemconcomp

Early-age hydration of accelerated low-carbon cements for digital fabrication

Arnesh Das *, Cedric Wenger, Lukas Walpen, Robert J. Flatt

Institute for Building Materials, ETH Zurich, Switzerland

A B S T R A C T

Digital fabrication processes with concrete offer several advantages compared to conventional processes, however, a major criticism with related concrete mixes has been with regard to their high cement paste content and consequent carbon footprint. One of the ways to address this is to reduce ordinary Portland cement (OPC) content in such mixes by using supplementary cementitious materials. This paper reports on such an approach for two different digital fabrication methods: digital casting system and 3D concrete printing. Results focus on the combined use of such low carbon blends with a calcium aluminate cement (CAC) based accelerator. Two such accelerators were studied: one being mainly crystalline based and the other mainly amorphous. Their performance is assessed at different temperatures. It is concluded that crystalline CAC is more suitable for applications above 20 °C while at temperature below 20 °C, amorphous CAC should be preferred. This paper also delves deeper into the effect of amorphous CAC on the hydration of tricalcium silicate present in OPC. It shows that the effect of amorphous CAC on that silicate depends on the OPC content of the system as well as on the type and amount of calcium sulfate used in the accelerator formulation.

1. Introduction

Research in digital fabrication with concrete has progressed greatly in the past years and as a result, interest in this field is also ever flourishing. There are many works that address the advantages and challenges associated with digital fabrication methods over conventional ones [1–6]. 3D concrete printing (3DP) and digital casting systems (DCS) are two of the well-established methods of digital fabrication [7–13].

In both cases, there remain however both materials science and process engineering challenges that need to be overcome. To begin, the material needs to be stable and pumpable for long periods of time without a significant flow loss. For this, it is common to retard the material to block the tricalcium silicate hydration and ensure enough open time [14,15]. Next, the material must be placeable according to process requirements. For instance, for 3D printing, the material needs to be extrudable with a yield stress sufficiently high for it to hold its shape after extrusion, whereas for digital casting, the material must be self-compacting so that it can easily fill the formwork [12,15]. Finally, for either process, the next requirement is for the material to build up strength rapidly. For this purpose, the material is often accelerated prior to the placing process and such a concept is referred to as 'set on demand' [16–22].

For ease of processing, digital concrete mixes are often associated with high cement paste content and a major criticism has been that such mixes are not the most sustainable. Furthermore, the set control of such mixes with most commercially available accelerators is easier to achieve when the ordinary Portland cement (OPC) content is relatively high. Another major limitation regards the size and volume of aggregates that can be incorporated into such mixes [23,24]. This is mainly due to processing and equipment limitations (pumping and inline mixing). Concerning the sustainability aspect, there are two ways of reducing the carbon footprint of the material – first, by increasing the volume of the aggregates and second, by substituting a part of the OPC by supplementary cementitious materials (SCMs). This study primarily focuses on the latter, and specifically on the strength build-up aspect, identifying suitable accelerators for such systems. Thereby, it brings an important addition to the currently still rather limited literature on the low carbon digital concrete mixes [25–28]. Information on process optimization and increased aggregate volume can be found elsewhere [29–32].

1.1. Strength development phases

Depending on the type of digital fabrication method, different strength development phases can be defined. This paper mainly focuses on the methods of digital casting and 3D printing. Fig. 1 shows the different strength development phases for the two processes. It is to be noted that the initial yield stress for the two processes are different.

For digital casting, three strength development phases may be identified (Fig. 1a).

* Corresponding author.
E-mail address: dasa@ethz.ch (A. Das).

https://doi.org/10.1016/j.cemconcomp.2025.105991
Received 13 September 2024; Received in revised form 31 January 2025; Accepted 15 February 2025
Available online 16 February 2025

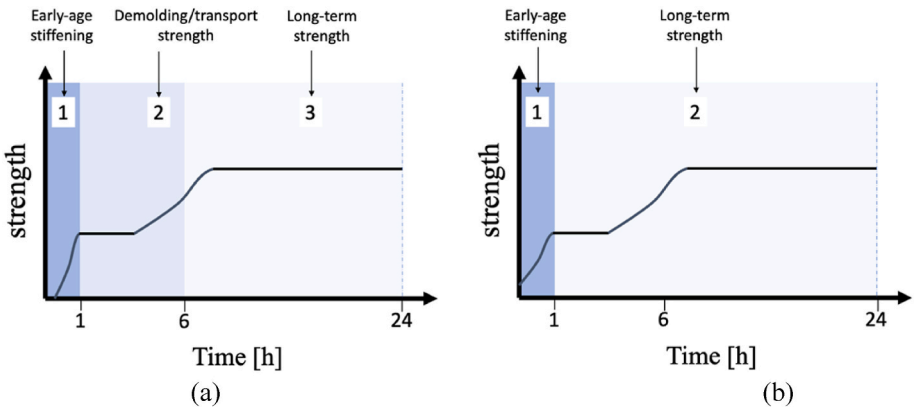

Fig. 1. Strength development phases for (a) Digital Casting System and (b) 3D concrete printing.

1. **Early-age stiffening**: One of the major advantages of the DCS is that the casting can be done in a continuous process in structurally optimized and low-cost thin formworks [12,13]. As the material is accelerated prior to the casting step, this allows having very limited build-up of hydrostatic pressure on the formwork. This strength evolution is critical for the fabrication phase.
2. **Demolding/transport strength**: The second stage of strength evolution mainly concerns the first 4–6 h. This characteristic of DCS can be exploited by the precast concrete industry. The current practice in the precast industry is that material is cast in standard formworks following the approach of batch processing and they are demolded about 10–24 h later. For DCS, since the material is accelerated before the casting process, it should be possible to demold/transport the elements earlier, provided the required strength (12–15 MPa as recommended by industry) is achieved. This can increase the production rate by about 50 % [12].
3. **Long-term strength**: Finally, the cast elements need to reach the required long-term strength properties, and this should be achievable through the hydration of OPC and SCMs. However, it is important to ensure that the accelerator type and formulation used does not adversely affect binder hydration in any way.

For 3D concrete printing, two strength development stages (Fig. 1b) may be identified.

1. **A) Early-age stiffening**: The strength build-up during the production phase is needed so that any extruded layer can sustain its own weight as well as that of the layers that would be subsequently placed over it. We distinguish two main approaches. First, an unsheared material, also referred to as a continuous brick, which stays in place after extrusion without accelerator, but may have a slower long-term strength gain. Second, the sheared material, this requires the addition of an accelerator to set as it is extruded and not flow out too much. Its initial strength gain rate is higher owing to the accelerator and therefore allows for a fast vertical building rate [15,16].**B) Buildability rate**: After deposition, the material needs to gain strength at a sufficient rate to avoid the lower layers from collapsing under the initial load. It is also understood that a too high initial strength gain may be detrimental to interlayer bonding, leading to the formation of so-called cold joints [15]. In contrast to DCS, there is no formwork to provide even a minimal support to the material, and the risk of cold joints is higher because the lower yield stress of DCS favors a better connection. However, in the case of DCS with thin formworks, a sufficient buildability rate is still important to keep the hydrostatic pressure to a minimum.
2. **Long-term strength**: After fabrication, the 3D printed structure would then have to fulfil the required long-term strength properties, and this is to be provided by the binder hydration. Again, it is important that this hydration, in most case in particular that of tricalcium silicate (C_3S), is not compromised due to use of certain accelerators or any other admixtures included in the mix design [18,19].

Among the various strength development phases, the first stage of 'early-age stiffening' is the most critical for either process, and having proper control over it can be even more challenging. There are numerous thickeners and accelerators that can be used for this. Viscosity modifying admixtures (VMAs) can contribute to an increase of yield stress but since they mostly influence the flocculation behavior, the required production strength would likely be difficult to achieve, particularly when a tall structure is to be printed/cast [15,33–35]. Common accelerators based on calcium chloride, calcium nitrate and C-S-H seeds are also available, but since they act on the silicate hydration, their benefit in providing the required 'early-age stiffening' in the first half hour to 1 h is limited [32–34]. Aluminate based accelerators based on either suspensions of calcium aluminate cement or aluminium sulfate rich solutions are more effective for the first stage and have been successfully used for 3D printing and DCS [11,15,16]. Such accelerators are also not affected by the retarders used for blocking silicate hydration [19]. Their performance is however influenced by temperature [36].

For DCS, the dosage of aluminate-based accelerators commonly used would not provide the required strength for demolding/transporting the elements. In order to obtain this strength, it is critical that the onset of silicate hydration happens well before the estimated demolding time. The fact that the base material mix is initially retarded to block the silicate hydration can make the situation trickier. Therefore, the correct dosage of retarder should be used so that the induction period of hydration after acceleration is not too long. Additionally, the temperature and both the type(s) and amount of SCM(s) used can also impact the onset point. In the case of 3D printing, the onset of silicate hydration is also critical for the stability of the printed structure, particularly for tall structures of height over 1m.

1.2. *Aluminate-silicate-sulfate balance*

For each of the strength development stages mentioned in the previous section, the aluminate-silicate-sulfate balance plays quite a critical role. It is well known that a high concentration of aluminate ions in the pore solution can adversely impact the C_3S hydration, which will eventually delay the onset point and also lower the long-term strength significantly [37–39]. Concerning the mechanism of the retarding action of aluminates on silicates, a major hypothesis is that the ions adsorb on to the surface of C_3S and block its dissolution [40,41]. Another hypothesis states that the presence of aluminate ions means that C-A-S-H precipitates instead of C-S-H and the former cannot act as seeds for further C-S-H growth, thus penalizing C_3S hydration [42]. A third

hypothesis talks about hydration products such as ettringite forming a barrier around the C_3S particles which inhibits dissolution [43]. However, this is not widely accepted as it was shown that even very low amounts of aluminate ions can heavily retard C_3S hydration [39].

One of the most common ways of avoiding the negative effect of aluminates is by using an additional calcium sulfate source. This helps to consume aluminate ions released in solution by precipitating them in ettringite which has a low solubility [44,45]. The type and amount of calcium sulfate used also plays a crucial role. The main calcium sulfate phases arranged in the decreasing order of their reactivity are hemihydrate ($CaSO_4.0.5H_2O$), gypsum ($CaSO_4.2H_2O$) and anhydrite ($CaSO_4$). If aluminate-based accelerators are used, the dissolution rate of the chosen calcium sulfate phase is also critical, particularly depending on the amount and rate at which the aluminates can dissolve [46]. Apart from this, it should be noted that a too high dosage of sulfates can lead to expansion issues [47,48].

In this paper, we have investigated the performance of calcium aluminate-based accelerators on blended cements. Further to this, an accelerator based on C-S-H seeds is also included. The performance of these accelerators is assessed at different temperatures. Studies are mainly based on progress of hydration, evolution of rheology immediately after acceleration and strength measurements. Based on this, we provide insights into mechanisms involved at early-age in the studied blended cement systems. Finally, conclusions are drawn about the suitability of such accelerator(s) for digital fabrication processes as DCS and 3DCP.

2. Materials and methods

2.1. Material

The OPC used for this study is CEM I 52.5R (Holcim Normo 5R). Two blended cement (BC) mixes were studied and for comparative purpose, an OPC mix was also included in the study. They have been named as BC70 (70 % OPC) and BC50 (50 % OPC). The SCMs used were limestone (LS; Nekafill 15, source: Kalkfabrik Nestal AG) and silica fume (SF; source: Holcim). The water to binder ratio of the studied cement paste mixes was 0.45. The composition of the BC mixes are as follows.

- BC70: 70%OPC +20%LS +10%SF
- BC50: 50%OPC +40%LS +10%SF

For studies on concrete mixes, apart from the above binders, limestone-based aggregates of size 0–4 mm and 4–8 mm were used. A commercially available PCE based superplasticizer called MasterGlenium ACE30 was used, while the viscosity modifying admixture (VMA) used was called MasterMatrix SCC2 (both sourced from Master Builders Solutions, Switzerland). An accelerator based on C-S-H seeds (X-seed STE54; Master Builder Solutions, Switzerland) was also used. For the BC concrete mixes, the water to binder ratio was 0.37. A lower water to binder ratio compared to the paste mixes was selected as the concrete mixes were prepared with superplasticizer, so the required self-compacting nature of the material was obtained. For the hydration studies on paste samples, the use of superplasticizer was avoided, and for it to be self-compacting, a higher water to binder ratio of 0.45 was selected. The difference in water to binder ratio for the paste was deemed okay since this has minimal effect on hydration kinetics.

Two different grades of CAC based accelerator were used for the study. One is crystalline based (CryCAC; Ciment Fondu, Imerys France) and the other is amorphous based (AmpCAC; LEAP FIT, Imerys France). The ratio of CryCAC to anhydrite was always fixed at 2:1. The commercially available amorphous based CAC already has the anhydrite included in it, the ratio of CAC to C$ being 1:1. A pure amorphous CAC (LEAP PURE, Imerys France) was also used which did not have any anhydrite included. Different ratios of AmpCAC and anhydrite (Anhy; Francis Flower) were tried with the LEAP PURE material. Additionally, hemihydrate (Hemi; FIXIT) was used as an alternative calcium sulfate source and the effect of inclusion of portlandite (CH; Sigma Aldrich) was also investigated. The CAC based accelerator pastes had a water to binder ratio of 0.38 and they were always retarded with tartaric acid (TA). The dosage of TA was 0.1 % and 0.3 % by weight of binder for the CryCAC and AmpCAC respectively.

Table 1
Mineralogical composition of used OPC and CryCAC using Rietveld analysis of XRD patterns. Phase quantities are normalized to 100 % of crystalline phases.

OPC		CryCAC	
Phase	Amount [% wt]	Phase	Amount [% wt]
C_3S	67.94	CA	63.14
C_2S	6.73	$C_{12}A_7$	3.81
C_3A	5.37	C_2S	8.85
C_4AF	11.13	C_2AS	2.78
Gypsum	7.25	C_4AF	21.43
Anhydrite	0.42		
Calcite	1.15		

Table 2
Specific surface area (SSA) and characteristic particle diameter D_{50} of used materials.

Material	SSA [m^2/g]	D_{50} [μm]
OPC	0.96	13.1
CryCAC	0.76	13.7
AmpCAC	0.82	12.4
Anhy	1.61	13.8
Hemi	1.52	18.8
LS	1.10	14.1
SF	20.20	0.8

Table 1 shows the mineralogical composition of used OPC and CryCAC using Rietveld analysis of XRD patterns. A Bruker D8 Advance Diffractometer which uses a cobalt anode for the generation of X-rays was used for the XRD measurement. The measurement was done on a range of 2θ values from 5-80°. The qualitative and quantitative phase analysis were then done in DiffracEva V4.3 and Profex 3.13.0 respectively. Phase quantities are normalized to 100 % of crystalline phases. With regard to AmpCAC (for which XRD analysis is not possible), it is known to have up to 95 % of amorphous calcium aluminate phases wherein the ratio of C to A is 1.7 (based on information received from producer/supplier, Imerys, France).

Table 2 shows information about BET specfic surface area (SSA) measurements as well as characteristic particle diameter (D_{50}) of the used materials. The BET specific surface area measurements of the materials used were done on instrument Micromeritics Tristar II 3020 using a BET multi-point nitrogen physisorption apparatus, while D_{50} was measured by laser diffraction after dispersion in isopropanol.

2.2. Mixing procedure

The preparation of the cement pastes was done in ambient lab temperature (20 °C). For the experiments done at 10 °C, all the raw materials were stored in a fridge at 7 °C, while the mixing happened in lab temperature.

The cement pastes were prepared using an IKA mixer which was operated at 500 rpm for 2 min. A delayed addition of the accelerator paste was followed, pertaining to the requirements of digital fabrication processes. The accelerator paste was added to the base mix, after at least 10 min of preparation of the latter. This was done to ensure that the base mix is well into the induction period. The dosage of accelerator was done by weight of binder. After addition to the base mix, it was mixed for an additional 1 min with the IKA mixer, again at 500 rpm.

For the concrete mixes, all the ingredients of the base mix were mixed for 5 min. The admixtures were added to the mixing water. The

Table 3
Summary of experimental methods followed and parameters studied in sections 3.1 and 3.2.

Section	Name	Experimental methods followed	Parameters studied
3.1	CryCAC vs AmpCAC	1.Rotational rheometry of paste samples at 16 °C and 23 °C. 2.6h compressive strength measurement of concrete mixes at 16–18 °C. 3.Isothermal calorimetry of paste samples at 16 °C.	1.Effect of CryCAC on early-age stiffening of OPC, BC70 and BC50 at 23 °C. 2.Effect of CryCAC and AmpCAC on early-age stiffening and demolding strength at 16 °C.
3.2	Influence of AmpCAC on C_3S hydration	1.Rotational rheometry of paste samples at 10 °C and 16 °C to study early-age stiffening. 2.Isothermal calorimetry of paste samples at 10 °C and 23 °C.	1.Effect of AmpCAC dosage. 2.Effect of AmpCAC to C$ ratio. 3.Effect of hemihydrate and calcium hydroxide

accelerator paste was subsequently added to the base mix after at least 10 min and mixed for an additional 1 min.

2.3. Rotational rheometry

The rheometer used was AntonPaar MCR 501. A parallel plate geometry was used, with the diameters of the upper and lower plates being 25 mm and 50 mm respectively. The test protocol followed was in accordance with Reiter et al. [49]. In a first period, the samples were pre-sheared with a constant shear rate of 50 s^{-1}, which resulted in a constant shear stress for all mixes before measuring strength evolution. As part of the second period, samples were subjected to a very small oscillatory shear strain (0.0005 %) with a frequency of 20 Hz. The evolution of storage modulus over time was then monitored for 20 min. The rheometry measurements were done at 10 °C, 16 °C and 23 °C.

2.4. Isothermal calorimetry and compressive strength

A TAMAir calorimeter was used to monitor the progress of hydration of the various accelerated mixes. It was operated at 10 °C and 16 °C. The compressive strength was tested for the concrete mixes on 15 cm cubes and the temperature range of curing/testing was 16–18 °C. The strength was measured at 6h after accelerator addition. Three cubes were cast for each tested mix and a machine from the company 'Testing GmbH' was used for testing the cubes.

2.5. Pore solution extraction and ICP-OES

Pore solution analysis was done for mix BC50 before and after acceleration. The pore solution was extracted by centrifugation and for the accelerated mixes, they were extracted immediately after acceleration. The centrifuge Allegra25R was used, and it was operated at 10000 rpm for 4 min.

The pore solutions were then immediately filtered using a 0.45 μm Nylon filter (Millipore). Samples were then diluted with 2 % nitric acid by weight. For each mix, samples were prepared with dilutions of 1:10 and 1:200 for the quantification of low-concentration elements (Al, Mg, Fe and Si) and high concentration elements (Ca, Na, K, S). For the ICP-OES measurement, the device Agilent 5100/5110 VDV was used.

3. Results and discussion

The first sub-section (3.1) shows results that help in identifying accelerator type/formulation that are suitable for digital casting and 3D printing, at two different temperature ranges: below and above 20 °C, a choice justified based on the accelerator behavior. First, we look at the 'early-age stiffening' performance of CryCAC and AmpCAC at 23 °C and 16 °C, followed by compressive strength measurements at 6h. The isothermal calorimetry results of the different mixes are also included which further validate the observations of the strength measurements. In section 3.2, we delve deeper into the effect of AmpCAC on C_3S hydration. A colour convention has been used for presenting the different results throughout the paper. The OPC, BC70 and BC50 mixes are represented by black, blue and green respectively.

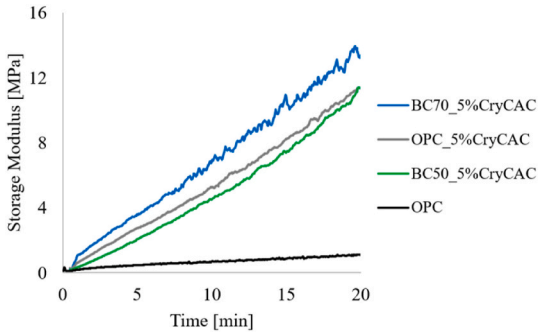

Fig. 2. Evolution of storage modulus over time for OPC and various blended systems at 23 °C. All mixes are accelerated with 5%CryCAC by weight of binder.

Table 3 shows an overview of sections 3.1 and 3.2 with regard to experimental methods followed and parameters studied in each case.

3.1. CryCAC vs AmpCAC at 23 °C and 16 °C

3.1.1. Early-age stiffening

Based on previous studies, it was concluded that at 23 °C, CryCAC is the preferred accelerator [36]. Fig. 2 shows the evolution of storage modulus over time for accelerated OPC and various blended systems at 23 °C. All accelerated samples show rates of strength gain that are similar and much larger compared to a non-accelerated OPC mix. This indicates that in the reported measured period (20 min), early-age stiffening with CryCAC is independent of the OPC or C_3S amount. Insights about the involvement of C_3S hydration in the first hour for OPC-CAC-C$ systems can be found in Das et al. [50].

Fig. 3 shows the evolution of storage modulus for various accelerated mixes at 16 °C, using both CryCAC and AmpCAC. As can be seen in Fig. 3a, AmpCAC shows a faster rate of strength build-up compared to CryCAC. For the latter, both BC70 and BC50 mixes show similar rate of strength development which again confirms the observation made at 23 °C. Also, AmpCAC shows a much faster rate of strength build-up for BC50 compared to that of BC70 which suggests that the OPC content of the system a role to play here. We look at this effect in more detail in section 3.2.1. Fig. 3b shows the evolution of storage modulus for mix BC50 at different dosages of AmpCAC. A higher dosage expectedly results in faster strength evolution which however does not scale linearly with the dosage. Indeed, at 2.5 % AmpCAC dosage, there is absolutely no increase in strength gain with respect to an unaccelerated OPC system. This points to the performance of AmpCAC having a dosage dependency with a threshold below which it does not seem to work.

3.1.2. Demolding/transport strength

Based on Fig. 3, it is clear that below 20 °C, AmpCAC is the preferred accelerator when it comes to obtaining the desired 'early-age stiffening' for a given digital fabrication process. Next, we look at the performance of the two accelerator types for the 'demolding/transport strength'. This is particularly critical for increasing productivity for digital casting processes.

Fig. 4 shows the compressive strength measurements for the various mixes at 6h after acceleration. Past experience showed that at 16–18 °C, the calcium aluminate accelerators alone struggled to reach demolding strengths at 6h. For this reason, experiments were conducted by adding

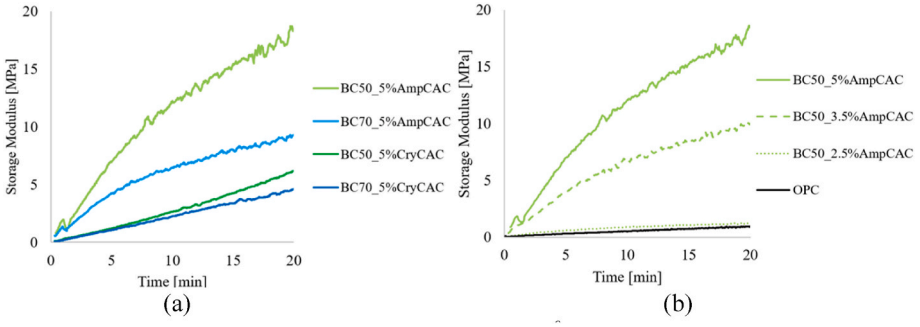

Fig. 3. Evolution of storage modulus over time at 16 °C for (a) BC70 and BC50 with 5 % dosage of both CryCAC and Amp CAC; (b) BC50 with different dosages of AmpCAC.

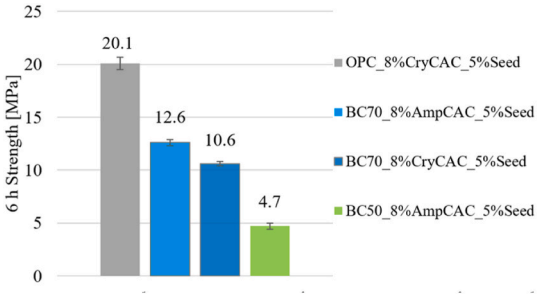

Fig. 4. 6h compressive strength measurements of concrete mixes after acceleration for the various mixes.

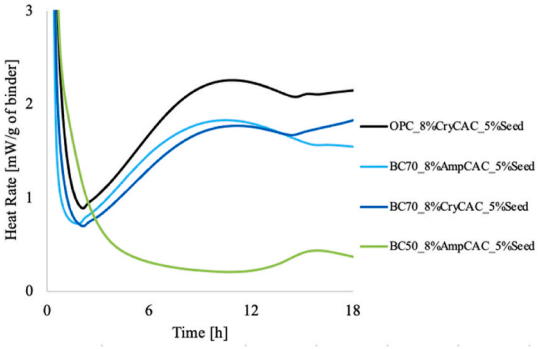

Fig. 5. Heat rates curves from isothermal calorimetry (at 16 °C) of the various accelerated mixes.

C-S-H seeds to mixes along with those calcium aluminate accelerators. A dosage of 5 % C-S-H seeds was selected, keeping in mind the lower temperature of the casting/curing conditions. In what follows, we report on the 6h strength of these mixes including both a calcium aluminate and a C-S-H seed accelerator. First, the OPC concrete mix shows a strength of 20.1 MPa with 8%CryCAC which is well above the required strength of 12–15 MPa for demolding/transporting the cast element. For mix BC70, an 8 % dosage of AmpCAC and CryCAC results in strength of 12.6 MPa and 10.6 MPa respectively. While this suggests that AmpCAC may be better than CryCAC below 20 °C, it is cannot deliver demolding strengths in the lower carbon blend BC50 at the same dosage (4.7 MPa at 6h).

Fig. 5 shows the heat rate curves from isothermal calorimetry (at 16 °C) of the various accelerated mixes. Both accelerated mixes of BC70 have essentially the same silicate peak of hydration, indicating that for BC70, neither accelerator has any adverse effect on tricalcium silicate hydration. The higher strength of BC70 accelerated with AmpCAC compared to that with CryCAC therefore most probably comes from the

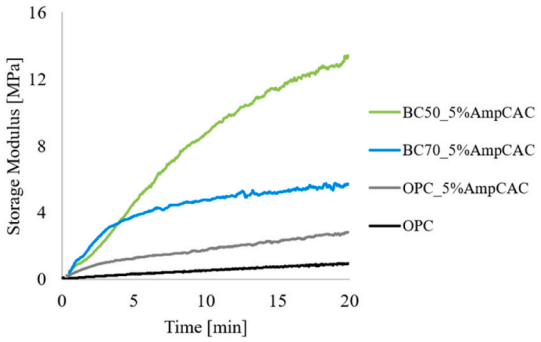

Fig. 6. Evolution of storage modulus over time for OPC and various blended systems at 10 °C. All mixes are accelerated with 5%AmpCAC by weight of binder.

fact that AmpCAC has higher amounts (90–95 %) of reactive component compared to CryCAC (55 % CA).

The lower peak of BC70 compared to OPC mix is expected as the silicate content of the mix is lower for the former. However, the silicate peak for accelerated BC50 is drastically lower and furthermore, its onset also takes place much later, after 9h instead of about 2h (as observed for the other mixes). This explains the particularly low 6h strength of BC50. It also indicates that in the case of BC50, an 8 % dosage of AmpCAC negatively affects the silicate hydration, most likely due to the aluminate ions in the pore solution. We delve deeper into this effect of AmpCAC on silicate hydration in section 3.2.

3.1.3. CryCAC vs AmpCAC

Before moving into the next section, we can draw some conclusions based on the results presented thus far. It has been established that AmpCAC appears to be the more appropriate accelerator to use at low temperatures, as it shows a more robust performance at temperatures below 20 °C. This is in line with previous reports that the dissolution rate of AmpCAC is not affected in the temperature range of 5–20 °C [51]. On the other hand, CryCAC is more suitable for temperatures above 20 °C. The open time of the respective accelerator pastes at these temperatures is also critical. It is particularly difficult to retard the AmpCAC and therefore, its application for digital fabrication processes is limited to low temperatures [36].

In terms of early-age stiffening at 16 °C, AmpCAC shows better performance compared to CryCAC. The strength results at 6h also confirms that AmpCAC is better for demolding/transporting the cast element. For OPC systems, AmpCAC up to a dosage of 8 % does not affect the silicate hydration but in the case of BC mixes, there seems to be an effect which likely depends on the OPC content of the mix.

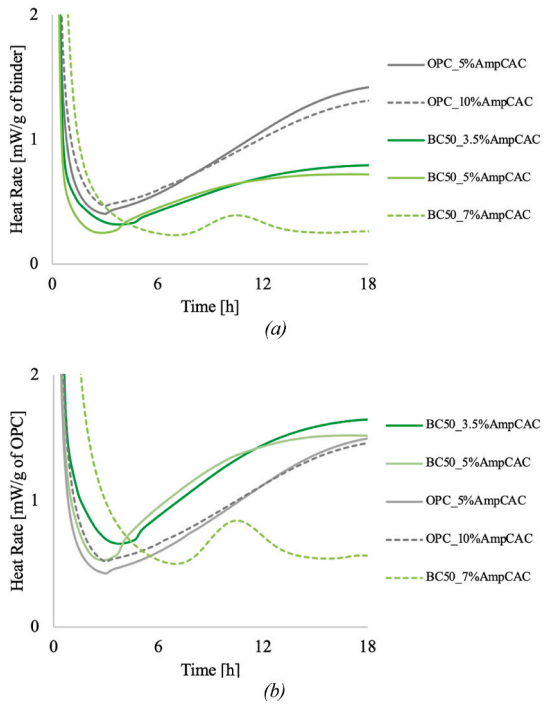

Fig. 7. Heat rates curves from isothermal calorimetry (at 10 °C) of OPC and BC50 accelerated with different dosages of AmpCAC, (a) heat rate is normalized by weight of binder, (b) heat rate is normalized by weight of OPC.

3.2. Influence of AmpCAC on C_3S hydration

At lower temperatures (10 °C), it was concluded in an earlier study that AmpCAC should be used [36]. Building on that, we examine the storage modulus evolution of various binders at 10 °C, all accelerated with 5 % AmpCAC. As can be seen from Fig. 6, the initial rate of strength build-up increases as the OPC content of the mix decreases. The reason for this is to be found in the fact that as the OPC content decreases, the overall sulfate content of the mix also decreases due to gypsum present in OPC. Indeed, a higher amount of calcium sulfate should promote a faster formation of ettringite and reaction of AmpCAC.

Based on Figs. 4–6, AmpCAC shows different performance depending on the OPC content of the system. Specifically, a significantly higher rate of strength build-up is observed with BC50 during the 'early-age stiffening period', while a significantly lower strength is obtained at 6h with that same binder. Also, from Fig. 5 it is clear that AmpCAC affects the hydration of C_3S, a topic that we deal with in more detail in the following section.

Fig. 7 shows the heat rates curves from isothermal calorimetry (at 10 °C) of OPC and BC50 accelerated with different dosages of AmpCAC. The silicate hydration proceeds normally for the OPC mixes up to an AmpCAC dosage of 10 % as well as for BC50 up to a dosage of 5 % by weight of binder. However, BC50 accelerated with 7 % AmpCAC shows a delayed silicate hydration with a significantly smaller peak. In particular, Fig. 7 (b) shows heat rate curves of the different accelerated mixes normalized by weight of OPC. As can be seen, up to a dosage of 5 % AmpCAC, the peak of silicate hydration is very similar to that of the accelerated OPC mixes. However, for the case of 7 % AmpCAC dosage, the peak is much lower and the onset of hydration happens much later, after 6h.

It is likely that this results from a flash set. Indeed, a very sudden change in rheology was observed for mix BC50_7%AmpCAC, which prevented it from being measured for strength build-up in the rheometer. To gain further insights into the behavior of AmpCAC in systems with low OPC content, the following factors were examined.

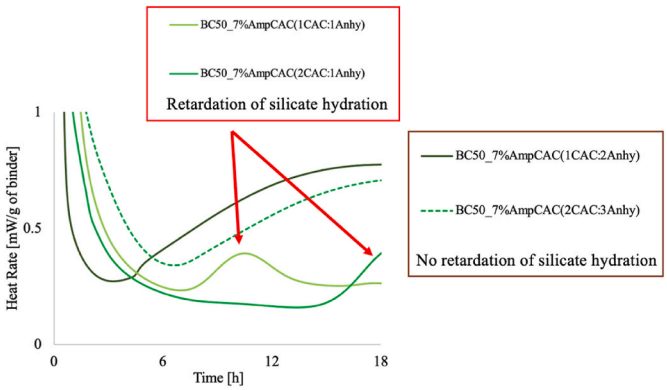

Fig. 8. Heat rates curves from isothermal calorimetry (at 10 °C) of mix BC50 with various ratios of CAC to C$. The accelerator dosage is 7 % by weight of binder.

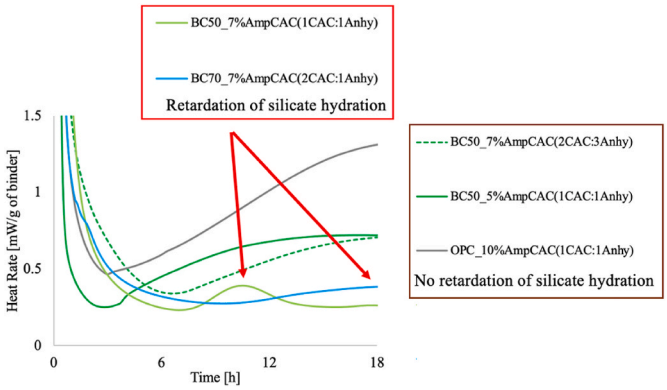

Fig. 9. Heat rate curves from isothermal calorimetry (at 10 °C) of different mixes at different CAC to C$ ratios. It is shown for different accelerator dosages.

- **CAC to C$ ratio**: The commercially available AmpCAC (LEAP FIT) has a CAC to C$ ratio of 1:1. Different ratios of CAC to C$ (with pure AmpCAC and anhydrite) were tested and their behavior was observed by calorimetry.
- **Hemihydrate**: Apart from the amount and type of calcium sulfates present in a system, the rate at which they dissolve could also have an effect in preventing the flash set. Therefore, hemihydrate was also tested instead of anhydrite.
- **Calcium hydroxide (CH)**: As reported by El Housseini, the addition of CH can help in the hydration of C_3S [52]. Thus, this compound was also added in the base mix and progress of hydration was assessed.

3.2.1. Effect of AmpCAC to C$ ratio

Fig. 8 shows the heat rate curves from isothermal calorimetry (at 10 °C) of mix BC50 with four different ratios of CAC to C$, all with the same accelerator dosage (7 % by weight of binder). The two samples with the higher anhydrite content (CAC to C$ ratio of 1:2 and 2:3) leads to the silicate hydration to proceed normally, while the two lower ones show the reaction to be inhibited (CAC to C$ ratios of 1:1 and 2:1).

Fig. 9 shows the heat rate curves from isothermal calorimetry (at 10 °C) of different mixes (OPC, BC70 and BC50) with various CAC to C$ ratios and for different accelerator dosages. There are two categories of mixes herein, one in which the C_3S hydration proceeds normally and the other in which it is retarded. In particular, mix BC50 with a 7 % accelerator dosage at 1:1 CAC to C$ ratio shows a strongly inhibited C_3S hydration, while this is not the case for the same accelerator dosage but with a CAC to C$ ratio of 2:3 ratio. If we keep the CAC to C$ ratio at 1:1 but reduce the accelerator dosage from 7 % to a 5 % dosage, the C_3S

Table 4
Ratios of pure AmpCAC to sulfates for studied mixes at different accelerator dosages. Mixes are arranged from top to bottom in increasing order of the ratio.

	Base mix name	Accelerator dosage [%]	Selected ratio of pure AmpCAC to C$	Ratio of pureAmpCAC to sulfates(mix)
No retardation	BC50	7	2:3	0.38
	BC50	5	1:1	0.43
	OPC	10	1:1	0.44
Retardation	BC50	7	1:1	0.52
	BC70	7	2:1	0.68

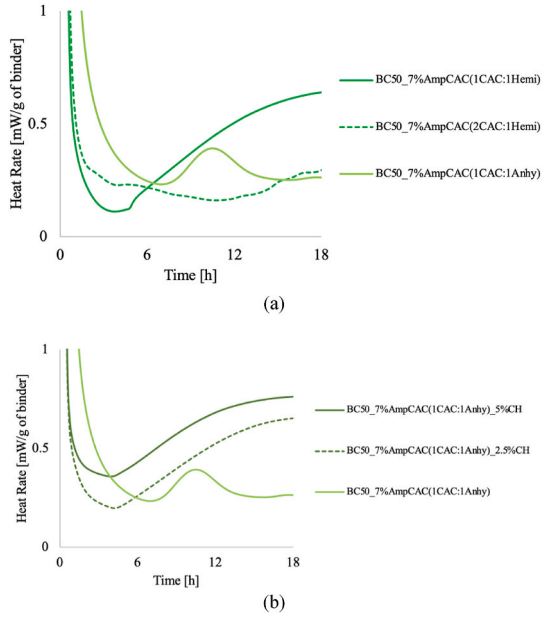

Fig. 10. Heat rate curves from isothermal calorimetry (at 10 °C) of mix BC50 with 7 % accelerator dosage (a) different ratio of AmpCAC to hemihydrate (b) Different dosages of CH addition in the base mix. These mixes are compared with BC50 with 7 % AmpCAC (1:1).

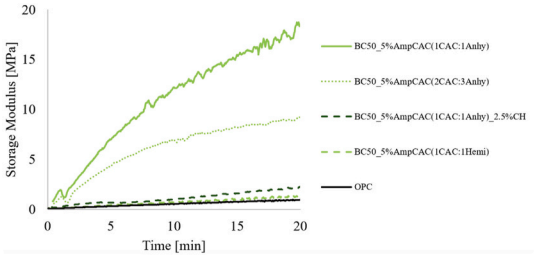

Fig. 11. Evolution of storage modulus at 16 °C for mix BC50 with different accelerator formulations.

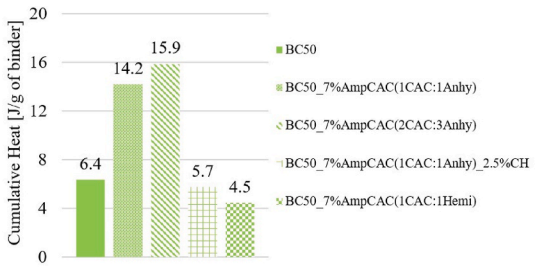

Fig. 12. Cumulative heat released for mix BC50 at 16 °C between 0.5 and 6h with and without acceleration.

hydration is not inhibited either. Also for a 1:1 CAC to C$ ratio but with OPC as a binder, no C_3S retardation is observed, even with a 10 % dosage. Apart from this, for an intermediate case with BC70, a 7 % dosage with 1:1 ratio does not affect silicate hydration but a ratio of 2:1 does. These results essentially show that the behavior of AmpCAC depends on the sulfate content of the whole system.

The OPC used in the study has a gypsum content of 7 % by weight. The gypsum from the OPC and the anhydrite from the accelerator paste contribute to the sulfate content of the entire system. The actual ratio of AmpCAC to sulfates in the system may be calculated based on Equation (1):

$$Sulfates_{mix} = Sulfates_{(OPC)} + Sulfates_{acc} \quad (1)$$

For the samples reported above, Table 4 shows the ratio of pure AmpCAC to total sulfates in the mix. Again, there are two categories of mixes, one in which silicate hydration progresses normally and one in which it is retarded. The last column reports the AmpCAC to sulfate ratio in the mix, including the OPC content, and this shows that both sample groups are separated around a threshold of that ratio between 0.44 and 0.52.

3.2.2. *Effect of hemihydrate (Hemi) and calcium hydroxide (CH)*

Fig. 10 shows the heat rate curves from isothermal calorimetry (at 10 °C) of mix BC50 with 7 % accelerator dosage. From Fig. 10 (a), it can be seen that an accelerator formulation based on AmpCAC to hemihydrate ratio of 1:1 does not affect the silicate hydration. However, if the ratio is changed to 2:1, then a retardation of C_3S hydration is observed. The retardation effect is even more pronounced than the case of 1:1 ratio of AmpCAC to anhydrite. This confirms further that both the sulfate content as well as the dissolution rate is critical. From Fig. 10b, it can be seen that CH addition helps the C_3S hydration to proceed normally. In fact, the hydration process is accelerated as CH dosage is increased from 2.5 % to 5 %. For the cases of CH addition, this was used to replace the respective amount of limestone in the mix.

3.2.3. *Early-age stiffening with hemihydrate (Hemi) and calcium hydroxide (CH)*

As previously mentioned, and as can be seen from Fig. 10, replacing anhydrite with hemihydrate and addition of CH do have a positive effect on the hydration of C_3S. However, for the purpose of digital fabrication, the early-age stiffening is equally important, which is why the effect of both hemihydrate and CH on strength build-up immediately after acceleration was checked with rheometry. Fig. 11 shows the evolution of storage modulus at 16 °C for mix BC50 with different accelerator formulations. A first observation is that with either hemihydrate or CH addition, there is no strength build-up whatsoever. It therefore seems that both block the hydration of AmpCAC. It can also be seen that at 5 % accelerator dosage (with anhydrite), the formulation with 1:1 ratio has a higher rate of strength build-up and higher ultimate storage modulus value (at the end of 20 min) compared to that of the 2:3 case. This is expected as pure AmpCAC content is higher in the former.

Fig. 12 shows the cumulative heat released for mix BC50 at 16 °C between 0.5 and 6h with and without acceleration. As can be seen, the cumulative heat released for mixes with either hemihydrate or CH addition are very similar to non-accelerated BC50. These mixes have significantly low heat releases at 6h, compared to the cases where immediate strength build-up was observed (1CAC:1Anhy and

Table 5
Pore solution concentrations of elements Al, S and Ca for mix BC50 with different accelerator formulations. The accelerated mixes have an AmpCAC dosage of 7 %.

Mix name	AmpCAC dosage [%]	C_3S retardation?	Concentration [mM]			Flash set?
			Al	S	Ca	
BC50	0	No	0.007	56.43	22.23	No
BC50_2.5%CH	7		0.004	55.37	16.59	
BC50_1:1Hemi			0.006	78.08	27.33	
BC50_1:1Anhy		Yes	6.476	61.54	3.88	Yes
BC50_2:1Anhy			19.33	35.55	1.15	

2CAC:3Anhy). It seems that both hemihydrate and CH block the hydration of AmpCAC and hydration proceeds similar to non-accelerated BC50. Due to limitations of calorimetry that needs time for temperature stabilization in the first 20–30 min, cumulative heat data was mainly examined from the 30-min mark.

3.2.3.1. Pore solution composition. To further confirm whether a flash set is occurring or not, ICP measurements were done on mix BC50 with four different accelerator formulations, all with 7 % accelerator dosage. Two of these samples delay the silicate hydration and two do not. Table 5 shows their pore solution concentrations for the key elements for Al, S and Ca. In the case of hemihydrate (1:1 ratio with pure AmpCAC) and CH addition (1:1 ratio of AmpCAC and anhydrite), the aluminate ion concentrations are very low and quite similar to the case of non-accelerated BC50. On the other hand, the mixes with anhydrite (1:1 and 1:2 ratio with AmpCAC) show much higher aluminate ion concentrations, suggesting that the retardation of C_3S hydration is due to a flash set. These results align well with the calorimetry curves of these mixes.

The sulfate concentrations for all mixes are very similar. For both cases of flash set, the measured high sulfate concentrations may be explained as follows. First, the alkali sulfates present in OPC can be expected to contribute to this. Second, it can be argued that flash set occurs within a few seconds while sample preparation for ICP takes few minutes. Therefore, this leaves enough time for the sulfates to dissolve after the flash set has happened. In any case, it should be underlined that in both cases of flash set, samples show much lower calcium concentrations compared to the other cases.

For the cases of 'no flash set', the pore solution composition is very similar to an OPC pore solution in the induction period. Based on these concentrations, GEMS [53] shows that the hydration products that can precipitate are ettringite, C-S-H and CH. On the other hand, for the 'flash set' cases, monosulphate is found to have positive saturation index values, indicating the possibility of its formation. However, it is to be noted that these thermodynamic calculations do not say anything about the kinetics of dissolution and precipitation.

3.3. Acceleration of BC50 with AmpCAC

It was seen that for mix BC50, with an AmpCAC to anhydrite ratio of 1:1 and an accelerator dosage of 7 %, that the hydration of C_3S is delayed and that much lower strength at 6h is obtained. This can be attributed to a case of flash set, which is supported by the high amount of aluminate ions in the pore solution, as reported in Table 2. This negative impact on C_3S hydration disappears when decreasing the AmpCAC to anhydrite ratio either to 2:3 or 1:2. In fact, a higher amount of anhydrite seems better for the silicate hydration. In the case of a 1:2 ratio, the onset point is similar to the non-accelerated BC50. It is likely that a higher amount of sulfates slows down the reaction of AmpCAC or accelerates the formation of ettringite, decreasing the concentration of aluminate ions in solution and preventing them from interfering with the hydration of C_3S.

El Housseini et al. [52] also studied the influence of AmpCAC on C_3S hydration whereby the ratio of AmpCAC to anhydrite was fixed at 1:1. Their study was about the effect of the molar ratio of C to A on the hydration of C_3S. They found that at high dosage (10 %), the AmpCAC with C to A ratio of 1.7 (similar to our study) adversely affected the silicates while the one with a ratio of 2.2 did not have any effect. They mentioned that a certain critical concentration of calcium in the pore solution is needed so that portlandite is supersaturated (which happened in the case of 2.2 ratio) and this can trigger the C_3S hydration. In the case of C/A ratio of 1.7, an enhancement of the degree of C_3S hydration was observed upon addition of 2 % CH, an observation which aligns well with our case. In our study, the cases where we see the silicate hydration being delayed also show low calcium concentrations, which has been attributed to a case of flash set. It is likely that calcium aluminate hydrates are forming as a consequence.

It was also seen that one can prevent the flash set and the retardation of C_3S hydration by using hemihydrate instead of anhydrite, as well as using CH in the base mix. In either case, calcium ions may be provided relatively quickly which should also accelerate the formation of ettringite and early-age strength build-up. However, there was absolutely no strength build-up observed for these cases, which may suggest that the afore-mentioned accelerator modification rather inhibit AmpCAC reaction rather than promote rapid and sustained ettringite formation. The cases of using AmpCAC with C/A ratio of 2.2 (with anhydrite) may be similar to that of using AmpCAC (C/A ratio of 1.7) with hemihydrate but the influence on early-age stiffening for the former has not been studied in El Housseini et al. [52].

The case of hemihydrate blocking the hydration of AmpCAC may bear similarities to the case of gypsum blocking C_3A hydration, whereby the formation of ettringite is also observed but understood to be a side effect responsible for keeping down aluminate concentration in solution owing to its low solubility.

When including CH in the base mix, additional calcium and hydroxide ions should be provided to the pore solution prior to acceleration (possibly up to CH saturation). This should a priori penalize the dissolution of both AmpCAC and anhydrite, attenuating their contribution to the overall hydration process and probably explaining that strength does not build-up in the case of CH addition.

Table 6
Summary of the applicability of the different blended cement systems and accelerator(s) that can be used for the two digital fabrication methods.

	Digital Casting (demold after 6h)			3D printing		
	Applicable:	Accelerator		Applicable:	Accelerator formulation	
		T < 20 °C	T > 20 °C		T < 20 °C	T > 20 °C
OPC	Yes	AmpCAC(1:1) C-S-H-seed	CryCAC(2:1)	Yes	AmpCAC(1:1)	CryCAC(2:1)
BC70	Yes	AmpCAC(1:1) C-S-H-seed	CryCAC(2:1)	Yes	AmpCAC(1:1)	CryCAC(2:1)
BC50	**No**	–	CryCAC(2:1)	Yes	AmpCAC(2:3)	CryCAC(2:1)

3.4. Selection of BC system and accelerator for different applications

Concerning the two blended cement systems investigated in the study, both can be used for either digital casting or 3D printing above 20 °C. In such cases, CryCAC would be the accelerator used and the performance in terms of early-age stiffening is similar for all of them. For digital casting in particular, the demolding/transport strength matters and hence, onset of silicate hydration as well peak value of hydration are critical, which directly depends on the OPC content of the system.

For temperatures below 20 °C, since the desired 'early-age stiffening' can be obtained with AmpCAC, mixes BC70 and BC50 should be applicable for 3D printing. For BC50 in particular, the AmpCAC to anhydrite ratio should be 2:3 so that the silicate hydration or in other words, the long-term strength is not compromised. In the case of digital casting, BC50 does not seem applicable at low temperatures as the required 6h strength could not be achieved. Also, for OPC and BC70, along with AmpCAC, C-S-H seeds may be added so that the silicate hydration is also accelerated. The addition of C-S-H seeds for 3D printing is however not a necessity since such accelerators do not have any effect during the 'early-age stiffening' period and their influence on the long-term hydration/strength is minimal. Table 6 summarizes the applicability of the different blended cement systems and accelerator(s) that can be used for the two digital fabrication methods. For the accelerator formulation, the number in the bracket signifies the recommended CAC to anhydrite ratio.

4. Conclusions

In this paper, we investigated the performance of calcium aluminate-based accelerators on blended cement systems. An accelerator additionally including C-S-H seeds is also included in the study. The performance of these accelerators has been assessed at different temperature. Based on the calorimetry, rheometry and strength measurements, the following conclusions can be drawn.

- For temperatures above 20 °C, blended cement mixes BC70 and BC50 may be used with CryCAC as the accelerator, for both digital casting as well 3D printing applications.
- For temperatures below 20 °C, AmpCAC would be the preferred accelerator. Blended cement mixes BC70 and BC50 can be used for 3D printing applications, however, for digital casting, only BC70 may be used. In all cases, it is recommended to include C-S-H seeds to reach rapid demolding times for digital casting at low temperatures.
- Depending on the OPC content of the system, the correct dosage of AmpCAC as well as its ratio to anhydrite need to be carefully chosen. In particular, it was found that for an accelerator dosage of 7 %, an AmpCAC to anhydrite ratio of 2:3 is safe to not adversely affect the silicate hydration of BC50. For the case of BC70, an AmpCAC to anhydrite ratio of 1:1 is safe while a ratio of 2:1 is not.
- The case of flash set and retardation of C_3S can be prevented by using hemihydrate instead of anhydrite in the accelerator formulation, and by including CH in the base mix. However, these cases do not show any early-age stiffening, rendering them useless for either digital casting or 3D printing.

Overall, this paper has highlighted possible pathways to reduce the carbon footprint of digital fabrication mixes both for digital casting and 3D printing. In most cases, decent performances can be obtained with 50 % less OPC, with low temperature digital casting only allowing 30 % reduction for the conditions considered in this paper. These promising routes do however require adequate selection of the accelerator and further research on this topic can be expected to render optimization more robust to enable large scale sustainable digital fabrication.

CRediT authorship contribution statement

Arnesh Das: Writing – original draft, Validation, Supervision, Methodology, Formal analysis, Conceptualization. **Cedric Wenger:** Validation, Methodology, Investigation, Formal analysis, Data curation. **Lukas Walpen:** Validation, Methodology, Investigation, Formal analysis, Data curation. **Robert J. Flatt:** Writing – review & editing, Supervision, Project administration, Funding acquisition, Formal analysis.

Declaration of competing interest

The authors declare that they have no known competing financial interests or personal relationships that could have appeared to influence the work reported in this paper.

Acknowledgements

This work was conducted as part of an Innosuisse project titled "Digital Casting System: Increased Productivity in Prefabrication", in collaboration with Dr. Ena Lloret-Fritschi, Assistant Professor, USI, Switzerland and Muller-Steinag Holding AG. The authors would like to thank Stefan Stocker (Müller Steinag Group) for the help in conducting the compressive strength measurements, and Prof Lloret-Fritschi and Cédric Domon (Director, Research and Development, Muller Steinag group) for the useful discussions about Digital Casting. The authors also acknowledge the support of Annette Rothlisberger from the Institute of Geotechnical Engineering, ETH Zurich for her help in carrying out the ICP measurements.

Data availability

The authors are unable or have chosen not to specify which data has been used.

References

[1] The Third Industrial Revolution, Economist (2012).
[2] R.A. Buswell, W.R. Leal de Silva, S.Z. Jones, J. Dirrenberger, 3D printing using concrete extrusion: a roadmap for research, Cement Concr. Res. 112 (2018) 37–49, https://doi.org/10.1016/j.cemconres.2018.05.006.
[3] M.S. Khan, F. Sanchez, H. Zhou, 3-D printing of concrete: beyond horizons, Cement Concr. Res. 133 (2020) 106070, https://doi.org/10.1016/j.cemconres.2020.106070.
[4] T. Wangler, E. Lloret, L. Reiter, et al., Digital concrete: opportunities and challenges, RILEM Tech Lett 1 (2016) 67–75, https://doi.org/10.21809/rilemtechlett.2016.16.
[5] H. Van Damme, Concrete material science: past, present, and future innovations, Cement Concr. Res. 112 (2018) 5–24.
[6] R.A. Buswell, W.R.L. da Silva, F.P. Bos, et al., A process classification framework for defining and describing Digital Fabrication with Concrete, Cement Concr. Res. 134 (2020) 106068, https://doi.org/10.1016/j.cemconres.2020.106068.
[7] N. Roussel, Rheological requirements for printable concretes, Cement Concr. Res. 112 (2018) 76–85, https://doi.org/10.1016/j.cemconres.2018.04.005.
[8] B. Khoshnevis, Automated construction by contour crafting—related robotics and information technologies, Autom. ConStruct. 13 (1) (2004) 5–19, https://doi.org/10.1016/j.autcon.2003.08.012.
[9] G. De Schutter, K. Lesage, V. Mechtcherine, V.N. Nerella, G. Habert, I. Agusti-Juan, Vision of 3D printing with concrete — technical, economic and environmental potentials, Cement Concr. Res. 112 (2018) 25–36, https://doi.org/10.1016/j.cemconres.2018.06.001.
[10] E. Lloret, A.R. Shahab, M. Linus, et al., Complex concrete structures: merging existing casting techniques with digital fabrication, Comput. Aided Des. 60 (2015) 40–49, https://doi.org/10.1016/j.cad.2014.02.011.
[11] E. Lloret Fritschi, L. Reiter, T. Wangler, F. Gramazio, M. Kohler, R.J. Flatt, Smart dynamic casting: slipforming with flexible formwork-inline measurement and control, HPCCIC Tromsø (2017). Published online 2017:Paper-no.
[12] E. Lloret-Fritschi, E. Quadranti, F. Scotto, et al., Additive digital casting: from lab to industry, Materials 15 (10) (2022) 3468, https://doi.org/10.3390/ma15103468.
[13] J. Burger, E. Lloret-Fritschi, F. Scotto, et al., Eggshell: ultra-thin three-dimensional printed formwork for concrete structures, 3D Print. Addit. Manuf. 7 (2) (2020) 48–59, https://doi.org/10.1089/3dp.2019.0197.
[14] D. Marchon, S. Kawashima, H. Bessaies-Bey, S. Mantellato, S. Ng, Hydration and rheology control of concrete for digital fabrication: potential admixtures and cement chemistry, Cement Concr. Res. 112 (2018) 96–110, https://doi.org/10.1016/j.cemconres.2018.05.014.

[15] L. Reiter, T. Wangler, N. Roussel, R.J. Flatt, The role of early age structural build-up in digital fabrication with concrete, Cement Concr. Res. 112 (2018) 86–95, https://doi.org/10.1016/j.cemconres.2018.05.011.
[16] L. Reiter, T. Wangler, A. Anton, R.J. Flatt, Setting on demand for digital concrete-principles, measurements, chemistry, validation, Cement Concr. Res. (2020), https://doi.org/10.1016/j.cemconres.2020.106047.
[17] A. Das, 3D Concrete Printing: Early-Age Strength Build-Up and Long-Term Durability, ETH Zurich, Switzerland, 2022. *PhD thesis*.
[18] A. Das, L. Reiter, T. Wangler, R.J. Flatt, Hydration control of ternary cements for digital fabrication with concrete, in: 2nd International RILEM Conference on Rheology and Processing of Construction Materials (RheoCon2 2019) and 9th International RILEM Symposium on Self-Compacting Concrete (SCC9 2019), 2019.
[19] A. Das, L. Reiter, S. Mantellato, R.J. Flatt, Early-age rheology and hydration control of ternary binders for 3D printing applications, Cement Concr. Res. 162 (2022) 107004, https://doi.org/10.1016/j.cemconres.2022.107004.
[20] J. Van Der Putten, M. Deprez, V. Cnudde, G. De Schutter, K. Van Tittelboom, Microstructural characterization of 3D printed cementitious materials, Materials 12 (18) (2019) 2993, https://doi.org/10.3390/ma12182993.
[21] N. Khalil, G. Aouad, K. El Cheikh, S. Rémond, Use of calcium sulfoaluminate cements for setting control of 3D-printing mortars, Constr. Build. Mater. 157 (2017) 382–391, https://doi.org/10.1016/j.conbuildmat.2017.09.109.
[22] H. Hu, J. Huang, T. Wang, et al., Impact of calcium sulfoaluminate cement on printability and early strength development of a slag-based 3D printing cementitious material, Constr. Build. Mater. 404 (2023) 133249, https://doi.org/10.1016/j.conbuildmat.2023.133249.
[23] T. Wangler, R. Pileggi, S. Gürel, R.J. Flatt, A chemical process engineering look at digital concrete processes: critical step design, inline mixing, and scaleup, Cement Concr. Res. 155 (2022) 106782, https://doi.org/10.1016/j.cemconres.2022.106782.
[24] R.J. Flatt, T. Wangler, On sustainability and digital fabrication with concrete, Cement Concr. Res. 158 (2022) 106837, https://doi.org/10.1016/j.cemconres.2022.106837.
[25] F. Boscaro, M. Palacios, R.J. Flatt, Formulation of low clinker blended cements and concrete with enhanced fresh and hardened properties, Cement Concr. Res. 150 (2021) 106605, https://doi.org/10.1016/j.cemconres.2021.106605.
[26] Y. Chen, S. Chaves Figueiredo, Z. Li, et al., Improving printability of limestone-calcined clay-based cementitious materials by using viscosity-modifying admixture, Cement Concr. Res. 132 (2020) 106040, https://doi.org/10.1016/j.cemconres.2020.106040.
[27] W.R.L. da Silva, M. Kaasgaard, T.J. Andersen, Sustainable 3D concrete printing with large aggregates, in: R. Buswell, A. Blanco, S. Cavalaro, P. Kinnell (Eds.), Third RILEM International Conference on Concrete and Digital Fabrication, Springer International Publishing, 2022, pp. 71–77, https://doi.org/10.1007/978-3-031-06116-5_11.
[28] BOD2 specifications | COBOD International. COBOD. https://cobod.com/solution/bod2/specifications/. (Accessed 9 August 2024).
[29] X. Wang, L. Jia, Z. Jia, et al., Optimization of 3D printing concrete with coarse aggregate via proper mix design and printing process, J. Build. Eng. 56 (2022) 104745, https://doi.org/10.1016/j.jobe.2022.104745.
[30] J. Xiao, Z. Lv, Z. Duan, S. Hou, Study on preparation and mechanical properties of 3D printed concrete with different aggregate combinations, J. Build. Eng. 51 (2022) 104282, https://doi.org/10.1016/j.jobe.2022.104282.
[31] T. Wangler, Y. Tao, A. Das, M. Mahmoudi, S. Gurel, R.J. Flatt, Aluminate 2K systems in Digital Concrete: process, design, chemistry and outlook, Cement Concr. Res. (2024), https://doi.org/10.1016/j.cemconres.2024.107644.
[32] S. Gurel, W.T. Chen, T. Wangler, E. Lloret Fritschi, R.J. Flatt, Scaling up in Digital Casting of concrete: towards industry integration, in: *4th RILEM International Conference On Concrete and Digital Fabrication*, Munich, Germany, 2024.
[33] K.H. Khayat, N. Mikanovic, 8 - viscosity-enhancing admixtures and the rheology of concrete, in: N. Roussel (Ed.), Understanding the Rheology of Concrete, Woodhead Publishing Series in Civil and Structural Engineering. Woodhead Publishing, 2012, pp. 209–228, https://doi.org/10.1533/9780857095282.2.209.
[34] J.J. Assaad, K.H. Khayat, Effect of viscosity-enhancing admixtures on formwork pressure and thixotropy of self-consolidating concrete, ACI Mater. J. 103 (4) (2006) 280–287.
[35] J. Assaad, K.H. Khayat, H. Mesbah, Assessment of thixotropy of flowable and self-consolidating concrete, ACI Mater. J. 100 (2) (2003) 99–107.
[36] Das A, Bousseau JN, Maach N, Flatt RJ. Effect of temperature on performance of calcium aluminate cement based accelerator. In: Further Reduction of CO2-Emissions and Circularity in the Cement and Concrete Industry, 16th International Congress on the Chemistry of Cement 2023-ICCC2023. Vol vol. 4. Thailand Concrete Association.
[37] A. Quennoz, K.L. Scrivener, Interactions between alite and C3A-gypsum hydrations in model cements, Cement Concr. Res. 44 (2013) 46–54, https://doi.org/10.1016/j.cemconres.2012.10.018.
[38] P. Suraneni, R.J. Flatt, Use of micro-reactors to obtain new insights into the factors influencing tricalcium silicate dissolution, Cement Concr. Res. 78 (2015) 208–215, https://doi.org/10.1016/j.cemconres.2015.07.011.
[39] E. Pustovgar, R.K. Mishra, M. Palacios, et al., Influence of aluminates on the hydration kinetics of tricalcium silicate, Cement Concr. Res. 100 (2017) 245–262, https://doi.org/10.1016/j.cemconres.2017.06.006.
[40] T. Chappex, K.L. Scrivener, The influence of aluminium on the dissolution of amorphous silica and its relation to alkali silica reaction, Cement Concr. Res. 42 (12) (2012) 1645–1649, https://doi.org/10.1016/j.cemconres.2012.09.009.
[41] B.R. Bickmore, K.L. Nagy, A.K. Gray, A.R. Brinkerhoff, The effect of Al(OH)4− on the dissolution rate of quartz, Geochem. Cosmochim. Acta 70 (2) (2006) 290–305, https://doi.org/10.1016/j.gca.2005.09.017.
[42] F. Begarin, S. Garrault, A. Nonat, L. Nicoleau, Hydration of alite containing aluminium, Adv. Appl. Ceram. 110 (3) (2011) 127–130.
[43] M. Gawlicki, W. Nocuń-Wczelik, Ł. Bąk, Calorimetry in the Studies of Cement Hydration, 2009, https://doi.org/10.1007/s10973-009-0158-5.
[44] Q. Xu, J. Stark, Early hydration of ordinary Portland cement with an alkaline shotcrete accelerator, Adv. Cement Res. 17 (1) (2005) 1–8, https://doi.org/10.1680/adcr.2005.17.1.1.
[45] D. Torréns-Martín, L. Fernández-Carrasco, M.T. Blanco-Varela, Conduction calorimetric studies of ternary binders based on Portland cement, calcium aluminate cement and calcium sulphate, J. Therm. Anal. Calorim. 114 (2) (2013) 799–807, https://doi.org/10.1007/s10973-013-3003-9.
[46] L. Xu, P. Wang, G. Zhang, Calorimetric study on the influence of calcium sulfate on the hydration of Portland cement–calcium aluminate cement mixtures, J. Therm. Anal. Calorim. 110 (2) (2012) 725–731.
[47] Bizzozero J. Hydration and dimensional stability of calcium aluminate cement based systems. Infoscience. doi:10.5075/epfl-thesis-6336.
[48] J. Bizzozero, C. Gosselin, K.L. Scrivener, Expansion mechanisms in calcium aluminate and sulfoaluminate systems with calcium sulfate, Cement Concr. Res. 56 (2014) 190–202, https://doi.org/10.1016/j.cemconres.2013.11.011.
[49] L. Reiter, T. Wangler, N. Roussel, R.J. Flatt, Distinguishing flocculation and hydration effects on the thixotropy of cement pastes, in: 8th International RILEM Symposium on Self-Compacting Concrete, Washington DC, USA, 2016.
[50] A. Das, L. Reiter, R.J. Flatt, Early-age hydration mechanism of ternary binders: quantitative relation between microstructure evolution and strength build-up, Cement Concr. Res. 170 (2023) 107191, https://doi.org/10.1016/j.cemconres.2023.107191.
[51] S. Berger, D. Tourlakis, S. Perrot, Ettringite accelerator in portland cement dominated systems: a comparison of different calcium aluminate technologies, International Conference on Calcium Aluminates (2022).
[52] S. El Housseini, Hydration and Durability of Fast Hardening Binders Incorporating Supplementary Cementitious Materials, EPFL, Switzerland, 2022. PhD thesis.
[53] B. Lothenbach, T. Matschei, G. Möschner, F.P. Glasser, Thermodynamic modelling of the effect of temperature on the hydration and porosity of Portland cement, Cement Concr. Res. 38 (1) (2008) 1–18, https://doi.org/10.1016/j.cemconres.2007.08.017.